

The Flow of a Model Suspension Fluid Past a Sphere

N. Phan-Thien,¹ R. Zheng,¹ and A. L. Graham²

Received March 22, 1990, final October 25, 1990

The paper is concerned with the flow of a dilute suspension of monosized spheroids past a sphere placed at the centerline of a cylindrical tube. The suspension is modeled by the transversely isotropic fluid model and the numerical solution is obtained by a time-dependent boundary element method. No steady-state solution to the problem was found. However, the amplitude of the long-time oscillations in the drag force on the sphere is only about 1% of its mean value at a solid volume concentration of 0.01 and an aspect ratio of 10 for the spheroids. The initial orientation of the microstructure has a small effect on the drag force: it can give rise to a $\pm 1\%$ variation in the drag force at large time.

KEY WORDS: Falling ball; suspension of fibers; boundary element method; Ericksen method.

1. INTRODUCTION

The flow of a fluid past a sphere has received a great deal of attention in the past. Much of this interest has been generated from the possibility of measuring the effective viscosity by observing the fall of precision spheres through the fluid of interest. The apparatus required is relatively simple to construct and the underlying theory for Newtonian fluids is well understood. When the fluid is non-Newtonian the problem is considerably more complex and the final analysis depends on the particular fluid model adopted.

Much of the theoretical studies of the non-Newtonian problem were based on perturbation and variational methods; a review of this is found

¹ Department of Mechanical Engineering, University of Sydney, Sydney, NSW 2006, Australia.

² Mechanical and Electronic Engineering Division, Los Alamos National Laboratory, Los Alamos, New Mexico 87544.

in Acharya *et al.*⁽¹⁾ Such results are limited to slightly non-Newtonian fluids or to inelastic generalized Newtonian fluids.⁽²⁾ Numerical studies using finite difference,^(3,4) finite element,⁽⁵⁻⁹⁾ and boundary element methods⁽¹⁰⁾ have also been attempted. Most recent numerical work concentrated on the uniform flow of the Oldroyd-B fluid past a sphere placed on the centerline of a cylindrical tube; the problem was posed as one of the benchmark problems for different numerical techniques in the 5th Workshop on Numerical Methods in Non-Newtonian Flows.⁽¹¹⁾ The quantity of interest to the experimenters is the drag coefficient χ defined by

$$\chi = F/F_N$$

where F is the drag force on the sphere and F_N is the corresponding drag force for a Newtonian fluid of the same (zero shear rate) viscosity in an unbounded body of fluid. Overall, there is an agreement between different numerical methods. They predict a drag reduction with increasing Weissenberg number (defined by $\lambda U/a$, where λ is the relaxation time, a is the sphere radius, and U is its velocity relative to the cylindrical tube); at a Weissenberg of 0.7, a drag reduction of about 25% was found. Experimental data on a polyacrylamide in glycerine solution⁽⁶⁾ confirmed the drag reduction and provided some degree of confidence in the numerical predictions.

In a recent paper, Milliken *et al.*⁽¹²⁾ presented some falling sphere data for a suspension of blunt-ended cylinders and chopped nylon fibers (of aspect ratio ≈ 19.8). The data strongly suggest that the falling sphere system can form the basis of a viscometer for these suspensions. In the recent Workshop in Dynamics of Concentrated Systems, Powell⁽¹³⁾ presented further data showing that the initial orientation of the fibers has a strong effect on the drag force on the sphere. Since the initial orientation of the fibers cannot be controlled to an arbitrary accuracy, it is desirable to know how much of the orientation effect is due to simply a change in the fluid viscosity, and how much is due to the nonlinear interaction between the fibers.

This paper attempts to analyze the uniform flow of a model suspension fluid past a sphere in a cylindrical tube. The numerical method used is the boundary element method, which has proved to be very effective in analyzing the same flow geometry, but with the Oldroyd-B model.⁽¹⁴⁾ The constitutive equation adopted is the transversely isotropic fluid (TIF) model.⁽¹⁵⁾ The connection between this model and the microstructure of the fluid was elucidated in Batchelor,⁽¹⁶⁾ Cox and Brenner,⁽¹⁷⁾ and Leal and Hinch.^(18,19) An equivalent constitutive equation was used in Lipscomb *et al.*⁽²⁰⁾ in their study of entry flow of fiber suspensions. The computational

method used in ref. 20, however, was a steady-state finite element technique. The existence of a steady-state solution in the entry flow problem has not yet been established.

The main conclusion drawn in this paper is that there is no steady-state solution to the problem. The amplitude of the oscillations in the drag force on the sphere is, however, no more than 1% of the mean value at long time observation. Furthermore, it is found that an uncertainty in the initial orientation of the microstructure can result in a variation of about $\pm 1\%$ in the drag coefficient. The effective viscosity inferred from the drag force on the sphere for the case where the aspect ratio is 20 agrees well with the data of Milliken *et al.*⁽¹²⁾ In addition, near the centerline behind the falling sphere and at long time (of the order 4 dimensionless time), the fibers tend to align themselves with the tube axis, a phenomenon that has been observed in experiments.

2. GOVERNING EQUATIONS

We consider the flow generated by a sphere falling along the centerline of a cylindrical tube containing a model suspension fluid. The radius of the sphere is a , and the radius of the tube is $2a$ (these are the dimensions recommended by the Fifth Workshop in Numerical Methods in Non-Newtonian Flows). In a frame of reference that is translated with the sphere, the sphere is at rest, the tube wall is seen moving with a constant velocity (the falling speed U of the sphere, but in the opposite direction of the falling sphere). Henceforth, all length scales are normalized with respect to a and velocities are normalized with respect to U ; the time is therefore made dimensionless with respect to a/U . Furthermore, the fluid far away from the sphere is seen moving rigidly with the tube, and all associated stresses are zero there. The two equations that we wish to solve are

$$\nabla \cdot \mathbf{u} = 0 \quad \text{and} \quad \nabla \cdot \boldsymbol{\sigma} = 0$$

subjected to the above-mentioned boundary conditions, in which \mathbf{u} is the velocity field and $\boldsymbol{\sigma}$ is the total stress field given by

$$\boldsymbol{\sigma} = -P\mathbf{1} + \mathbf{S}$$

where P is the hydrodynamic pressure, $\mathbf{1}$ is the unit tensor, and \mathbf{S} is the "extra" stress.

The simplest properly invariant theory of anisotropic fluids is the transversely isotropic fluid (TIF) model proposed by Ericksen.⁽¹⁵⁾ In this model the microstructure of the fluid is characterized by a unit vector field \mathbf{p} , which evolves in time according to a certain law. The stress generated by

the microstructure is a tensor-valued function of this unit vector field and the strain rate tensor.

Jeffery⁽²¹⁾ considered the motion of a rigid spheroid suspended in a Newtonian fluid. He showed that the spheroid translated with the fluid velocity and rotates according to

$$\frac{D\mathbf{p}}{Dt} = \mathbf{W} \cdot \mathbf{p} + \frac{R^2 - 1}{R^2 + 1} (\mathbf{D} \cdot \mathbf{p} - \mathbf{D} : \mathbf{p}\mathbf{p}) \quad (1)$$

where $D(\cdot)/Dt$ is the material derivative, $\mathbf{W} = [(\nabla\mathbf{u})^\dagger - \nabla\mathbf{u}]/2$ is the vorticity tensor, $\mathbf{D} = [(\nabla\mathbf{u})^\dagger + \nabla\mathbf{u}]/2$ is the strain rate tensor, the dagger denotes a transpose operation, R is the aspect ratio of the spheroid, and \mathbf{p} is a unit vector along the major axis of the spheroid. Note that as $\dot{\mathbf{p}} \cdot \mathbf{p} = 0$, the magnitude of \mathbf{p} is preserved in this time evolution. If \mathbf{p} is initially a unit vector, then it remains a unit vector at all time.

Batchelor,⁽¹⁶⁾ Cox and Brenner,⁽¹⁷⁾ Leal and Hinch,^(18,19) among others, considered a dilute suspension of monosized rigid spheroids and obtained the volume-averaged stress using Jeffery's solution. They showed that the TIF model is the appropriate continuum description of the suspension. In this case the unit vector field \mathbf{p} is simply the unit vector along the axis of the spheroid, and the bulk stress generated by the microstructure is given by⁽¹⁸⁾

$$\mathbf{S} = 2\eta\mathbf{D} + 2\eta\Phi\{A\mathbf{D} : \mathbf{p}\mathbf{p}\mathbf{p}\mathbf{p} + B(\mathbf{D} \cdot \mathbf{p}\mathbf{p} + \mathbf{p}\mathbf{p} \cdot \mathbf{D}) + C\mathbf{D} + d_R F \mathbf{p}\mathbf{p}\} \quad (2)$$

where η is the viscosity of the solvent, Φ is the volume fraction, d_R is the rotational diffusivity of the spheroids, and A , B , C , and F are material constants depending on the aspect ratio of the microstructure. The asymptotic values of A , B , C , and F are tabulated in Table I.

In this paper, we are concerned with a dilute suspension of macrosized fibers (large aspect ratio) so that the diffusivity can be set to zero. The

Table I. Asymptotic Values of A , B , C , and F

Asymptotic limits	A	B	C	F
$R \rightarrow \infty$ (rodlike)	$\frac{R^2}{2(\ln 2R - 1.5)}$	$\frac{6 \ln 2R - 11}{R^2}$	2	$\frac{3R^2}{\ln 2R - 0.5}$
$R = 1 + \delta, \delta \ll 1$ (near-sphere)	$\frac{395}{147} \delta^2$	$\frac{15}{14} \delta - \frac{395}{588} \delta^2$	$\frac{5}{2} \left(1 - \frac{2}{7} \delta + \frac{1}{3} \delta^3 \right)$	9δ
$R \rightarrow 0$ (disklike)	$\frac{10}{3\pi R} + \frac{208}{9\pi^2} - 2$	$-\frac{8}{3\pi R} + 1 - \frac{128}{9\pi^2}$	$\frac{8}{3\pi R}$	$-\frac{12}{\pi R}$

size of the fibers must, however, be considerably smaller than the radius of the falling sphere for the suspension to be treated as a continuum. It is interesting to note that Milliken *et al.*⁽¹²⁾ found that falling spheres smaller than the length of the fibers give the same average viscosity as much larger spheres. The implication of the dilute assumption for a suspension of fibers is that $\Phi R^2 \ll 1$. However, experimental studies by Milliken *et al.*⁽¹²⁾ showed that the dilute regime extends to $\Phi R^2 \approx 50$. Note that, from (1),

$$\frac{D \mathbf{pp}}{Dt} = \mathbf{W} \cdot \mathbf{pp} - \mathbf{pp} \cdot \mathbf{W} + \frac{R^2 - 1}{R^2 + 1} (\mathbf{D} \cdot \mathbf{pp} + \mathbf{pp} \cdot \mathbf{D} - 2 \mathbf{D} : \mathbf{pppp})$$

This is identical to the constitutive equation adopted by Lipscomb *et al.*⁽²⁰⁾ for solving the 4:1 entry flow problem. As a consequence of their closure assumption $\mathbf{D} : \langle \mathbf{pppp} \rangle = \mathbf{D} : \langle \mathbf{pp} \rangle \langle \mathbf{pp} \rangle$ [their Eq. (24)], where the angular brackets denote an ensemble average, their $\langle \mathbf{pp} \rangle$ is equivalent to \mathbf{pp} in our notation and thus the constitutive equation adopted in ref. 20, although written in terms of $\langle \mathbf{pp} \rangle$, is mathematically the same as our constitutive equation.

The TIF model, represented by (1), (2), is quite successful in describing certain qualitative features of suspensions. It predicts that both the shear stress and the first normal stress difference are linear in the shear rate $\dot{\gamma}$ in a simple shearing flow. In addition, the stresses are functions of $\dot{\gamma}t$, where t is the time. These features have been observed in experiments⁽²²⁾ with suspensions of polystyrene spheres (diameter ranging from 40 to 50 μm) in a silicon oil. However, the stresses are periodic in time, which corresponds directly with the Jeffrey orbits executed by the spheroids⁽²¹⁾ and has been observed in dilute suspensions.⁽²³⁾ Specifically, in a simple shearing flow with shear rate $\dot{\gamma}$, it can be shown that \mathbf{p} is periodic in time:

$$p_1 = (\alpha \cos \omega t + \beta \sin \omega t)/P$$

$$p_2 = \left(\frac{\zeta}{2 - \zeta} \right)^{1/2} \frac{\beta \cos \omega t - \alpha \sin \omega t}{P}$$

and

$$P = \left[(\alpha \cos \omega t + \beta \sin \omega t)^2 + \frac{\zeta}{2 - \zeta} (\beta \cos \omega t - \alpha \sin \omega t)^2 \right]^{1/2}$$

where α and β are constants related to the initial values of \mathbf{p} , and the frequency ω is given by

$$\omega = \frac{1}{2} [\zeta(2 - \zeta) \dot{\gamma}^2]^{1/2}, \quad \zeta = \frac{2}{R^2 + 1}$$

which is proportional to the magnitude of the shear rate.

The stresses are moments of \mathbf{p} , and there is no *a priori* estimate of how fast (or how slow) they are varying in time in a complex flow. For example, the plot of $p_1(t) p_2(t)$ in a simple shearing flow is shown in Fig. 1; note that it varies rapidly at certain time interval.

The instantaneous viscosity is defined by the ratio of the shear stress to the shear rate; it is given by

$$\eta_{\text{eff}} = \eta [1 + \Phi(B + C + 2Ap_1^2(t) p_2^2(t))]$$

The leading asymptotic terms (at large aspect ratio) of the preceding equation are $\eta(1 + \Phi C)$. For a better estimate of the effective shear viscosity, the time average value of $p_1^2(t) p_2^2(t)$ should be used. At an aspect ratio of $R = 10$, this gives an effective viscosity of $\eta_{\text{eff}} = \eta(1 + 4.8\Phi)$, and when $R = 20$, this yields $\eta_{\text{eff}} = \eta(1 + 6.2\Phi)$ irrespective of the initial orientations of the fibers (the initial configurations of the fibers only affect the third significant figures in the coefficients of Φ when the aspect ratio is less than 20). The results obtained by Ganani and Powell⁽²⁴⁾ in shear flow for rods having $R = 25$ yield $\eta_{\text{eff}} \approx \eta(1 + 10\Phi)$, which is in reasonable agreement with the predicted value of $\eta(1 + 7\Phi)$ at this aspect ratio. The TIF constitutive theory is therefore not inconsistent with experimental data in simple shearing flows.

The fact that the kinetics is periodic in time in the simple shearing flow suggests that there is no guarantee of having a steady-state solution in complex flows, at least in those that have a shear flow component in parts of the flow domain (the 4:1 entry flow is one such example). The numerical

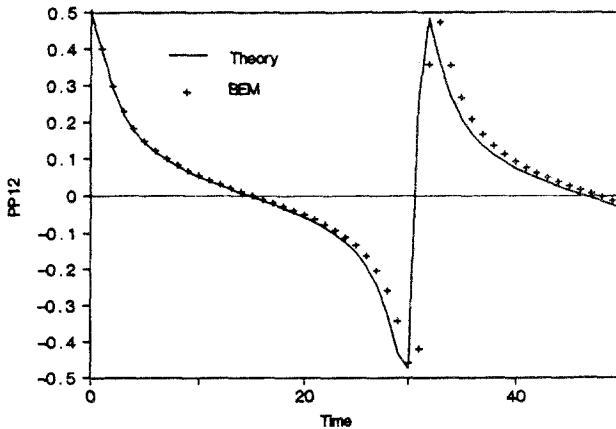


Fig. 1. The moment $p_1(t) p_2(t)$ in a simple shearing flow of shear rate $\dot{\gamma} = 1$. The aspect ratio of the spheroid is $r = 10$, $\Phi = 0.01$, and initially $p_1 = p_2 = 0.5$.

method adopted to solve the TIF model must necessarily be a time-dependent method; furthermore, the time integration scheme must be robust enough to handle fast-varying stresses.

3. NUMERICAL SIMULATION AND RESULTS

The numerical method adopted is the boundary element method (BEM), which has been described in several papers^(10,25) and need not be repeated here in detail. In essence, the method solves a series of linear problems, each with a known body force (the domain integrals of the extra non-Newtonian stresses) until convergence is achieved. The difference between the previous BEM^(10,25) and the present scheme is the constitutive equations chosen and the method for computing the extra stresses. Sugeng and Tanner⁽¹⁰⁾ employed a streamline scheme, whereas a time integration scheme similar to that used in ref. 25 is employed here.

A streamline scheme can be developed here by first defining a vector \mathbf{q} that evolves in time according to

$$\dot{\mathbf{q}} = \mathcal{L}\mathbf{q} \quad (3)$$

where \mathcal{L} is an "effective" velocity gradient yet to be determined and the dot denotes the material time derivative. Let \mathbf{p} be the unit vector along \mathbf{q} , i.e.,

$$\mathbf{p} = \frac{\mathbf{q}}{q} \quad (4)$$

Thence

$$\dot{\mathbf{q}} = \dot{\mathbf{q}} \cdot \mathbf{p} = q\mathcal{L} : \mathbf{p}\mathbf{p}$$

and thus \mathbf{p} evolves in time according to

$$\dot{\mathbf{p}} = \mathcal{L}\mathbf{p} - \mathcal{L} : \mathbf{p}\mathbf{p}$$

This is identical to (1) if the "effective" velocity gradient tensor is given by $\mathcal{L} = \mathbf{L} - \zeta\mathbf{D}$, where $\zeta = 2/(R^2 + 1)$. Along a streamline the material derivative is simply the arc length derivative. Thus, given the boundary conditions at the entry of the flow domain and the kinematics, Eq. (3) can be integrated along the streamline. The unit vector field \mathbf{p} can be found from Eq. (4), and hence the stress tensor can be found from Eq. (2). This scheme was implemented in the current BEM. However, we found that it is not very robust, especially with a fine mesh when the kinematics have yet

to converge. Streamline crossing may occur in this case, leading to a divergence of the numerical results.

The time integration scheme (fourth-order Runge-Kutta), which is based on integrating Eq. (3) using available current information, is much more robust and was adopted in this study. Another advantage of the time integration method is its ability to cope with recirculatory regions; actually there are none in this problem.

We first test the numerical method for the unbounded flow of the Newtonian fluid past a sphere. In this case, the drag force on the sphere is simply $6\pi\eta Ua$, where η is the fluid viscosity, and U is the speed of the sphere. Here, χ should be exactly one. This problem results in a set of integral equations of the first kind (prescribed velocities on the boundary of the sphere, and the boundary tractions are sought after). Integral equations of the first kind can lead to a set of ill-posed algebraic equations upon discretization,^(26,27) while integral equations of the second kind yield a set of well-conditioned algebraic equations. Table II shows the numerical results for different mesh sizes (all uniform). When the program runs in single-precision mode (32-bit arithmetics), roundoff errors become important if the number of boundary elements is greater than 72, and the error steadily worsens. However, in double-precision mode (64-bit arithmetics), the rate of convergence is nearly quadratic in the number of elements, up to 360 elements.

Table II. Comparison of Results from Different Meshes for the Unbounded Flow of the Newtonian Fluid Past a Sphere^a

Number of boundary elements	χ	Error (%)
20	0.9974664	0.253
30	0.9988667	0.113
40	0.9993498	0.0650
50	0.9995726	0.0427
60	0.9996946	0.0305
72	0.9998025	0.0197
90	0.9998735	0.0126
120	0.9999288	0.00712
180	0.9999683	0.00317
240	0.9999821	0.00179
300	0.9999885	0.00114
360	0.9999922	0.000786

^a The exact result for χ is 1.

We have also carried out similar numerical experiments for the flow past oblate and prolate spheroids. In both cases the aspect ratio of the polar radius to the equatorial radius varies from 0.1 to 0.5. The ill-conditioning problem does not arise in double-precision arithmetics, and in all cases we obtain five significant figures in accuracy when the number of boundary elements is about 300.

Next, we test the robustness of the time integration scheme in the simple shearing flow. Figure 1 shows good agreement between the boundary element results and the exact results. The slight disagreement in the region of $t = 30$ is due to our large chosen time step ($\Delta t = 0.05$). With smaller time steps, the agreement between the numerical results and the exact solution improves at the expense of computing time.

We consider now the flow past a sphere placed at the center of a tube. This problem does not result in a set of integral equations of the first kind, and we can expect the problem to be well-behaved numerically. Different meshes with varying degrees of coarseness used in the study are listed in Table III and shown in Figs. 2a–2c; only the results from the finest mesh are reported here. The half-length of the cylinder is chosen to be $6a$ and the ratio of sphere-to-cylinder radius is 0.5. This cylinder half-length is chosen based on the kinematics obtained for the Newtonian and the Oldroyd-B fluids.⁽¹⁴⁾ It will be seen that a half-length of $6a$ is also adequate for the suspensions.

The boundary conditions are:

1. At the entry of the flow domain ($z = -6a$) plug flow conditions are applied, where the axial velocity $u = U$, the radial velocity $v = 0$.
2. Along the tube wall ($r = a$), $u = U$ and $v = 0$.
3. Along the centerline ($r = 0$), symmetry boundary conditions apply, where $v = 0$ and the axial traction $t_x = \sigma_{rz} = 0$.
4. On the surface of the sphere, $u = 0 = v$.

Table III. Summary of the Boundary Element Meshes Used for the Calculations

Name	Boundary elements	Domain cells	Smallest boundary element length
M1	52	240	0.262a
M2	96	640	0.157a
M3	132	1456	0.105a

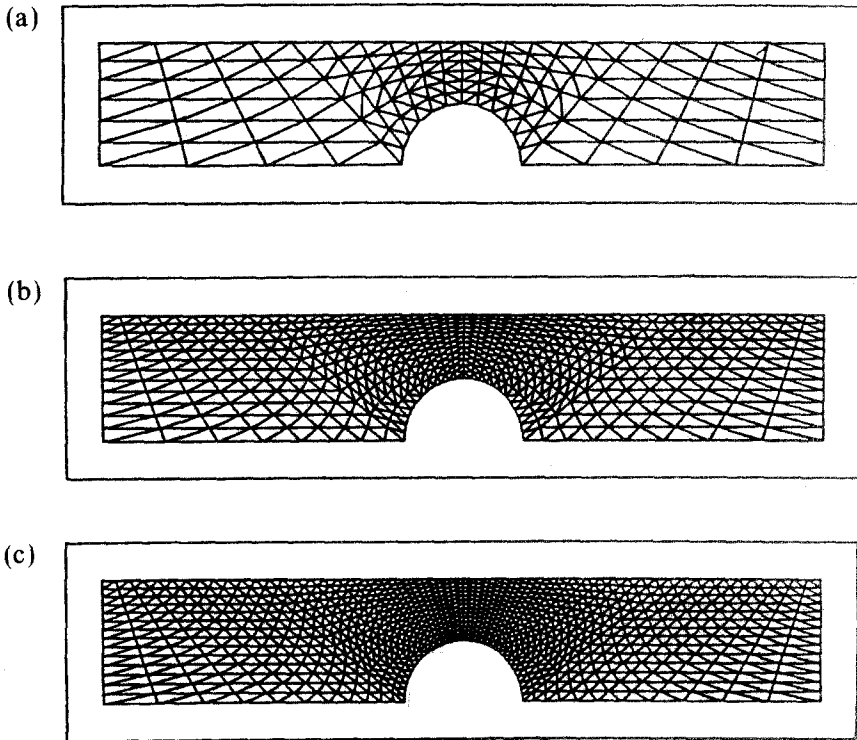


Fig. 2. Meshes for the calculations. (a) M1, (b) M2, (c) M3.

5. At the outlet of the flow domain ($z = 6a$), the axial traction is set to zero (no net force action on the fluid), and the radial velocity $v = 0$.

In addition, all stress components are set to zero and \mathbf{p} is set to a known vector initially.

When the wall effects are considered, the Stokes drag for the Newtonian fluid can be estimated from the value of unbounded case using the Bohlin formula⁽²⁸⁾ (R is the tube radius here):

$$\chi = [1 - 2.10444(a/R) + 2.08877(a/R)^3 - 0.94813(a/R)^5 - 1.372(a/R)^6 + 3.87(a/R)^8 - 4.19(a/R)^{10}]^{-1} \quad (5)$$

For the geometry under consideration Eq. (5) predicts $\chi = 5.923$. (The theory of Haberman⁽²⁸⁾ predicts the value to be 5.970. Recent careful finite element⁽⁹⁾ and boundary element⁽¹⁴⁾ studies show this value to be 5.943.)

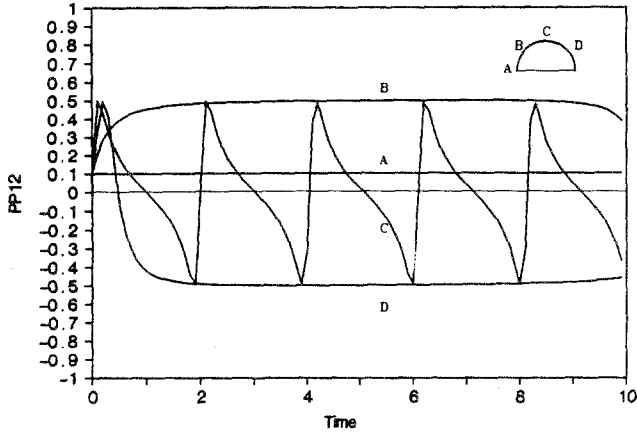


Fig. 3. The moment $p_1(t) p_2(t)$ as a function of time at different locations on the surface of the sphere. $R = 10$, $\Phi = 0.01$. Initially, the spheroids are aligned at an angle of $\theta = 45^\circ$ to the tube axis.

Our numerical results give $\chi = 5.777$, 5.900 , and 5.919 from mesh M1, M2, and M3, respectively, for the Newtonian case.

For the TIF model, which is the primary focus of this paper, we find that the kinetics is periodic in time. Figure 3 shows the moment $p_1(t) p_2(t)$ at different locations on the surface of the sphere as a function of time for

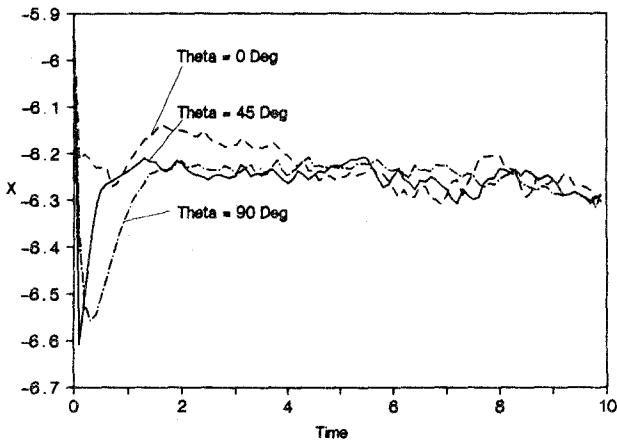


Fig. 4. The drag force (normalized with respect to $6\pi\eta Ua$) on the sphere as a function of time for three different initial configurations of the spheroids, $\theta = 0^\circ$ (parallel to the tube axis), $\theta = 45^\circ$ (this corresponds to a random distribution of the spheroids), and $\theta = 90^\circ$ (perpendicular to the tube axis). The aspect ratio of the spheroids is $R = 10$, and the volume fraction is $\Phi = 0.01$. The long-time average ($t > 4$) value of χ is 6.26 and its standard deviation is about 1%. This is translated into an effective viscosity of 1.058η for the suspension.

a spheroid aspect ratio of 10. At point A, the front stagnation point on the sphere surface, the local shear rate is zero, and $p_1(t) p_2(t)$ is seen to be independent of time. The local shear rate is highest at point C on the sphere surface; the curve $p_1(t) p_2(t)$ also has the highest frequency at this location. This corresponds to the results obtained in a simple shearing flow: the kinetics is periodic in time with a fundamental frequency that is proportional to the magnitude of the shear rate.

The traction on the surface of the sphere is also a periodic function of time, with a frequency that depends on the local shear rate. The drag force on the sphere is the area integral of the traction, and it should contain a spectrum of frequencies. Figure 4 shows this clearly for three different initial configurations of the spheroids, from $\theta = 0^\circ$ (aligned with the tube axis) to $\theta = 90^\circ$ (perpendicular to the tube axis). The case of $\theta = 45^\circ$ corresponds to a random distribution of the spheroids (on the average). At first sight, these curves appear random in time. However, upon Fourier transforming of the curves, we find that there is one dominant frequency at $\pi/2$ (note that the frequency is normalized with respect to U/a). Other frequencies contribute about equally to the spectrum, as Fig. 5 shows. This flat frequency spectrum makes the plot of the drag force against time appear random.

Other important features from Fig. 4 are worth mentioning. First, the amplitude of the unsteady component of the drag force is only about 1% of the mean value at long time observation ($t > 4$), given the initial configuration of the spheroids. Second, not knowing the precise initial configuration of the spheroids can result in about $\pm 1\%$ uncertainty in the

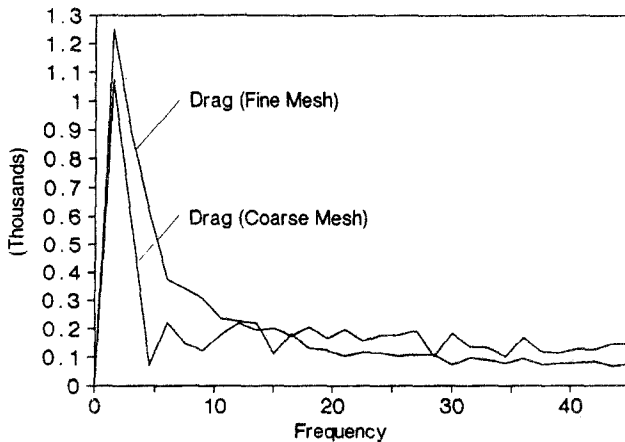
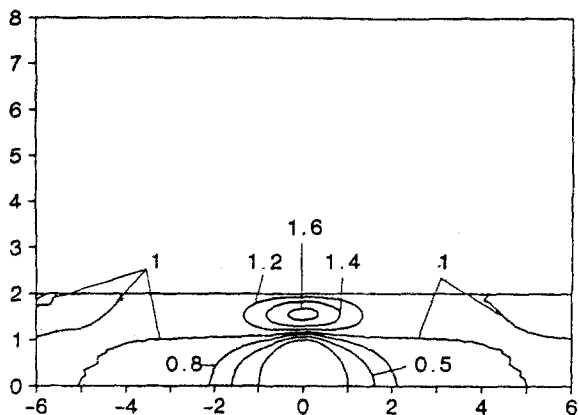
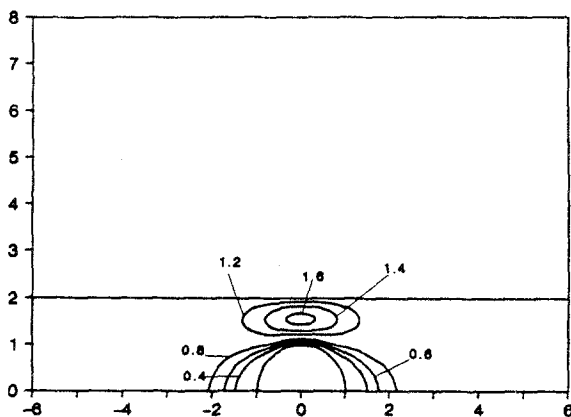


Fig. 5. The power spectrum of the drag force where $\theta = 45^\circ$. Except for a prominent peak at $\pi/2$, the power spectrum of the drag force is essentially flat.

drag force. That is, the long-time ($t > 4$) average values of the drag forces are only weakly dependent on the original orientation of the fibers. (The long-time mean value of χ is $\bar{\chi} = 6.26$, with a variation of 0.05 about the mean value, or about 1%, for different initial orientation of the fibers.) From the long-time average value of χ , and taking the wall effects into account, the effective viscosity of the suspension can be calculated to be 1.058η , which compares well with the shear viscosity value of 1.048η .



(a)



(b)

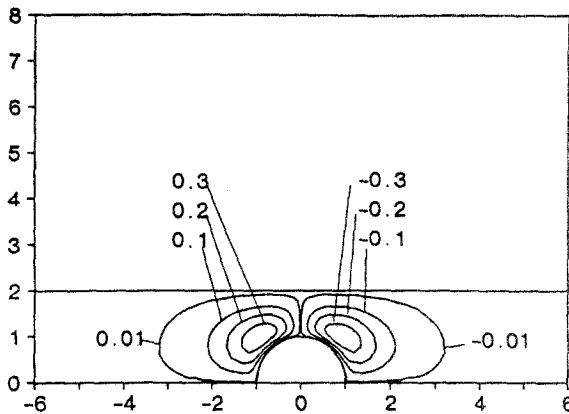
Fig. 6. Contours of axial velocities at $t = 10$, (a) Newtonian, (b) non-Newtonian; $R = 10$, $\Phi = 0.01$; initially, the spheroids are aligned perpendicular to the tube axis ($\theta = 90^\circ$). A few typical contour values are given.

At low volume concentration, the drag force should be proportional to the volume fraction [cf. (2)]. Thus, the effective viscosity found by the falling sphere method will be given by

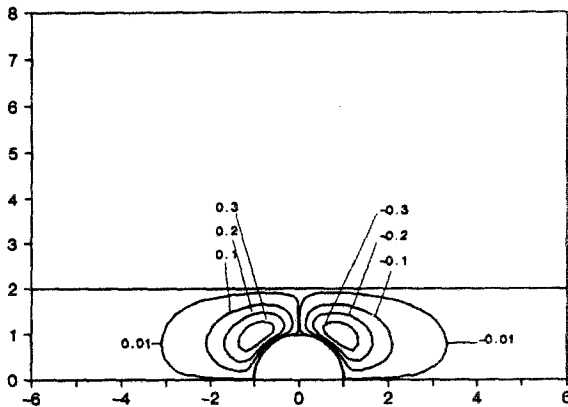
$$\eta_{\text{eff}} = \eta(1 + 5.8\Phi)$$

for a dilute suspension of rigid spheroids of aspect ratio 10.

The kinematics is similar to Newtonian kinematics, in contrast to the viscoelastic case, where a shift in the velocity contours was found^(6,10); this justifies our choice of the cylinder half-length of $6a$. In Figs. 6a and 6b, contours of the axial velocities are displayed, and in Figs. 7a and 7b, contours



(a)



(b)

Fig. 7. Contours of radial velocities at $t=10$; (a) Newtonian, (b) non-Newtonian; the parameters are given in Fig. 6. A few typical contour values are given.

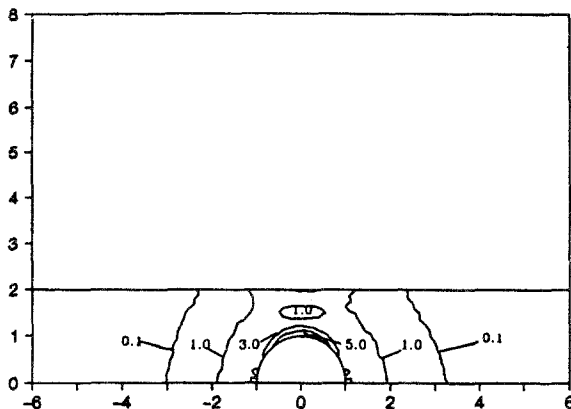


Fig. 8. Contours of maximum shear stress at $t = 10$. The parameters are given in Fig. 6. A few typical contour values are given. Highest shear stress occurs in the polar region of the sphere, where the polar angle is $\pi/2$.

of radial velocities are displayed. These non-Newtonian contours are similar to the Newtonian contours and are symmetric about the plane $x = 0$. This symmetry is not present in the viscoelastic flow.^(6, 11)

The contours of the maximum shear stress and the first normal stress difference are shown in Figs. 8 and 9, respectively. Most of the shearing action is confined to the polar region of the sphere.

The evolution of the orientation of the microstructure along the tube is shown in Figs. 10a-10f at different times. In these figures, \mathbf{p} is represented

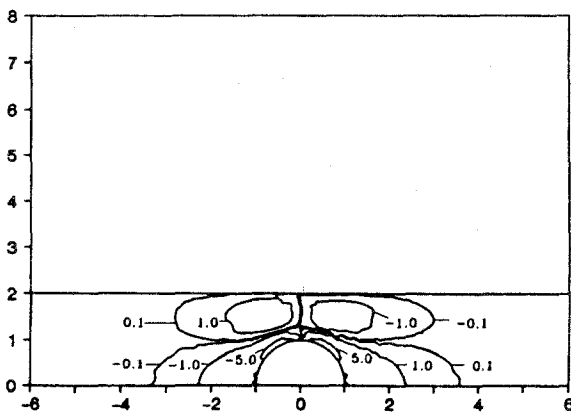


Fig. 9. Contours of the first normal stress difference N_1 at $t = 10$. The parameters are given in Fig. 6. A few typical contour values are given.

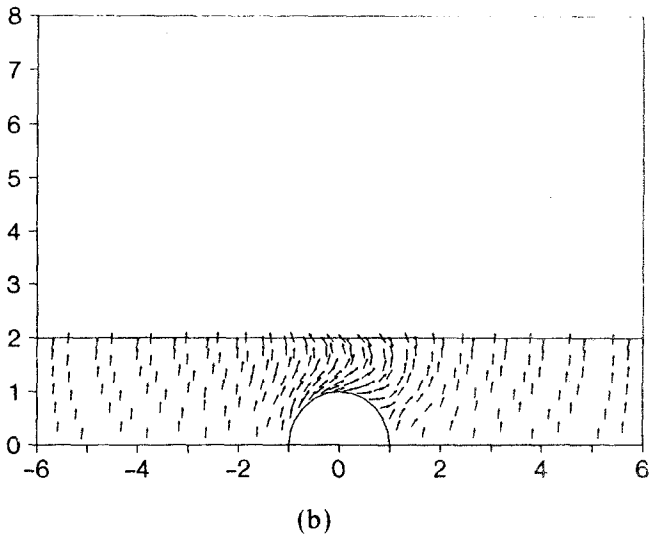
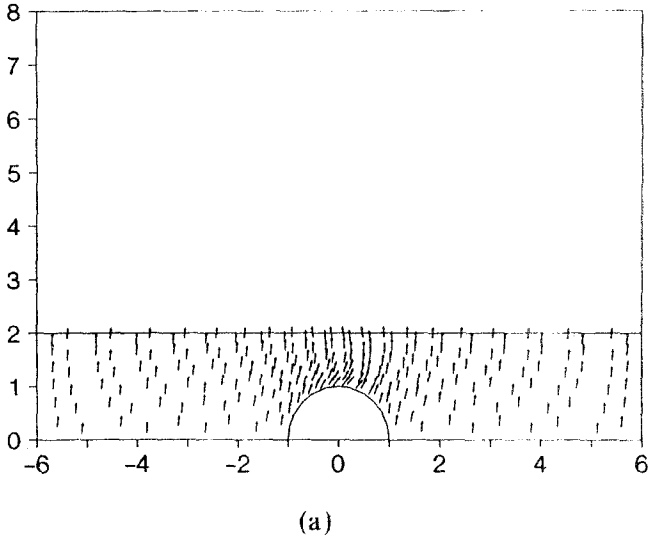


Fig. 10. The orientation of the microstructure. The parameters are given in Fig. 6. (a) $t = 0.1$, (b) $t = 0.5$, (c) $t = 1.0$, (d) $t = 1.5$, (e) $t = 2.0$, (f) $t = 2.5$.

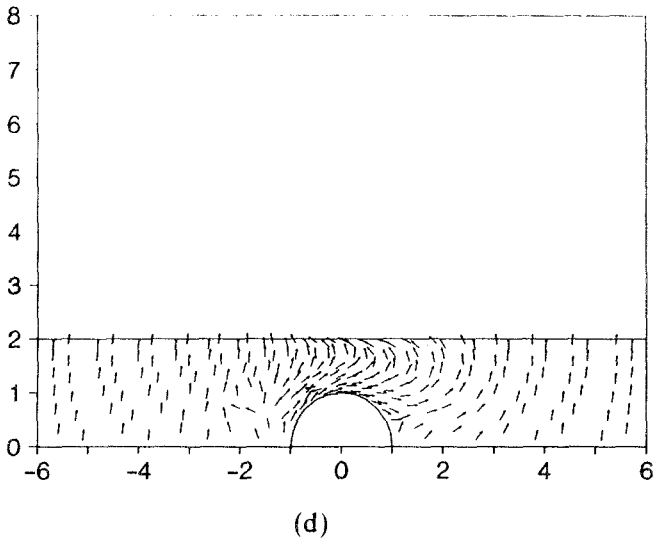
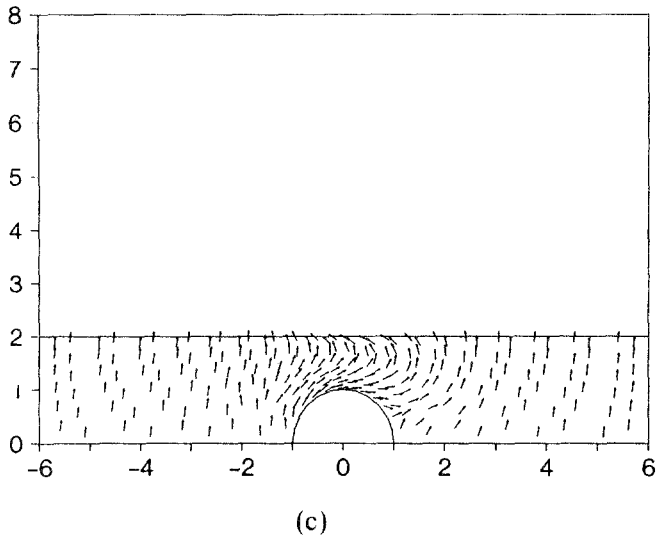


Fig. 10. (Continued)

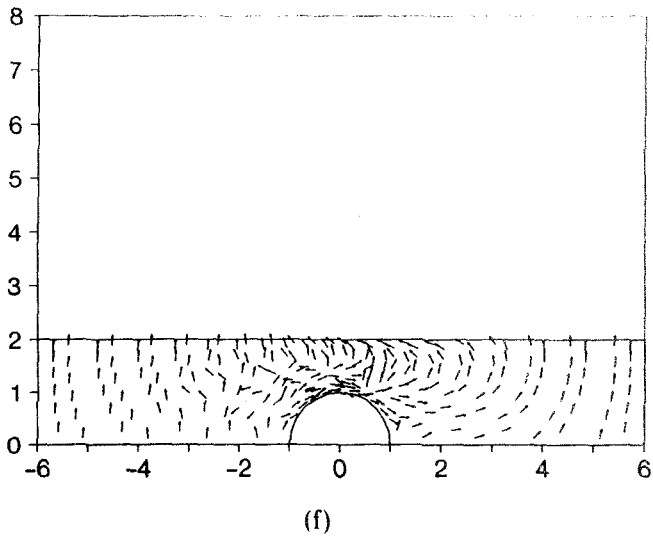
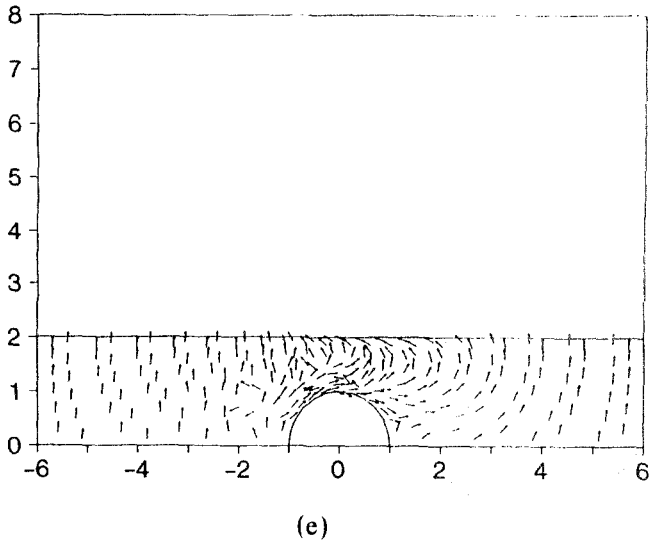


Fig. 10. (Continued)

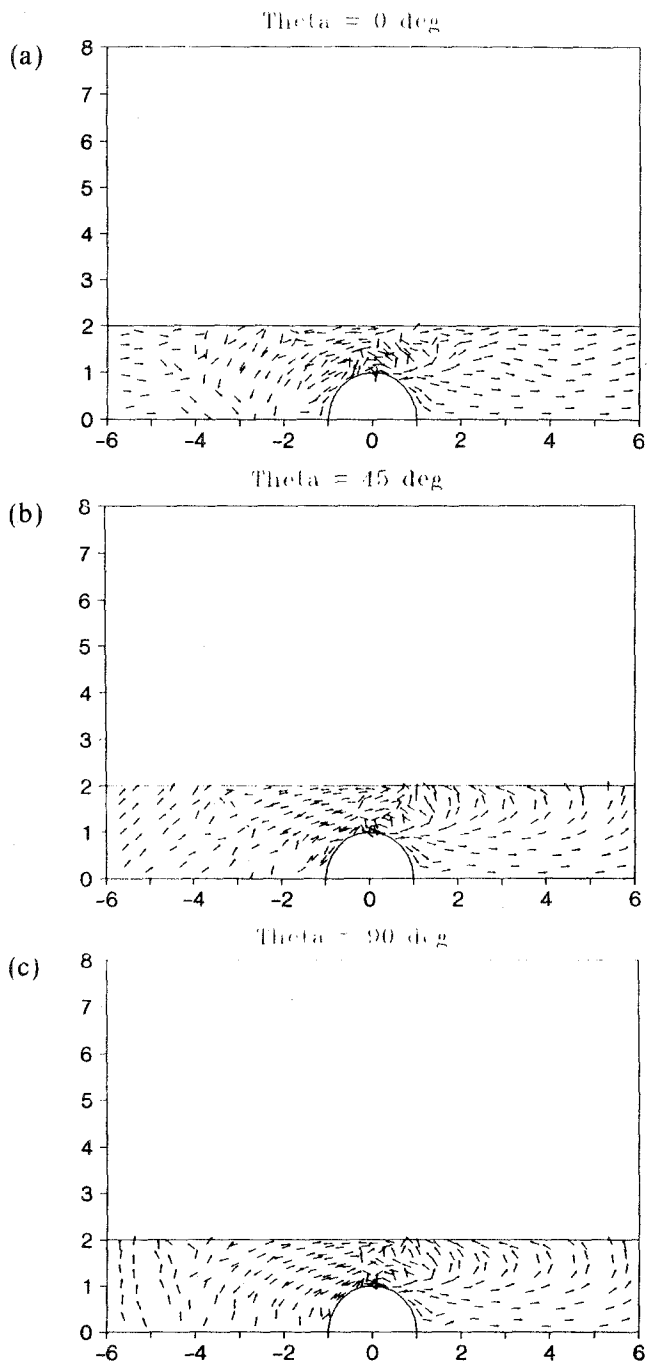


Fig. 11. The orientation of the spheroids at time $t=5$. The parameters are given in Fig. 6. (a) $\theta=0$, (b) $\theta=45^\circ$, (c) $\theta=90^\circ$, where θ is the initial angle that \mathbf{p} makes with the tube axis. Note that the fibers behind the sphere align with the axis.

by an arrow. It is seen that the major disturbances in the microstructure occur in the layer between the sphere and the tube, extending to about one sphere diameter upstream and downstream of the sphere. These disturbances can be quite severe: \mathbf{p} can flip its direction across a narrow layer of fluid ($\approx 0.1a$). This boundary layer occurs in the middle of the flow field and can cause difficulty in any analytical attempt at solving flows of suspensions.

It is most interesting to find that at large time (of the order >4) the spheroids tend to align themselves with the tube axis in the downstream wake region near to the tube axis regardless of their initial configurations (refer to Figs. 11a–11c). This tendency has been observed (unpublished data) with semiconcentrated systems. The falling ball, therefore, may be used as a device to partially align fibers. A physical explanation of this phenomenon is that the flow along the centerline in the downstream region of the sphere is extensional in nature; see, for example, ref. 14. Such a flow is capable of aligning the fibers well.

We also have some numerical data for suspensions of fibers with aspect ratio of 20. The drag force is plotted against time for the cases where $\theta = 0^\circ, 45^\circ, 90^\circ$ in Fig. 12. It is clear that the flow is unsteady. The long-time average value of χ and its standard deviation are 6.98 and 1%, respectively. This yields an effective viscosity of about 1.18 after applying the wall correction. This value compares well with the experimental value (≈ 1.23) for a random suspension of fibers (aspect ratio 19.8),⁽¹²⁾ as shown by Fig. 13. In this figure, the specific viscosity $\mu_r - 1 = \eta_{\text{eff}}/\eta - 1$ is plotted

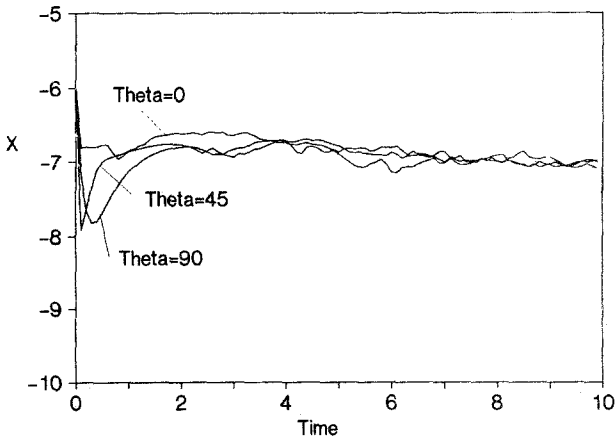


Fig. 12. The drag force (normalized with respect to $6\pi\eta Ua$) on the sphere as a function of time for spheroids with aspect ratio $R = 20$. The volume fraction is $\phi = 0.01$. The long-time average value for χ is 6.98, and its standard deviation is 1%. This is translated into an effective viscosity of 1.18η .

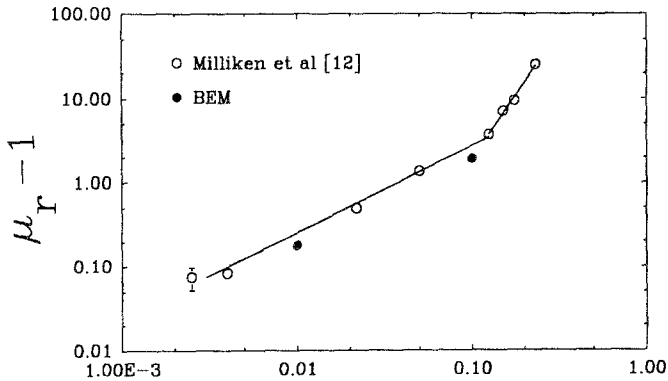


Fig. 13. Specific viscosity versus volume fraction. The data are from Milliken *et al.*⁽¹²⁾ The solid lines are the lines of best fit through the data and the vertical bar represents experimental errors. At low volume fraction, the experimental data show that the specific viscosity is proportional to the volume fraction; the coefficient of proportionality is estimated to be 28.5.⁽¹²⁾ The numerical results predict a coefficient of proportionality of 18.

against the volume fraction. The solid lines represent the lines of best fit through the data. At low volume fraction, the specific viscosity is proportional to the volume fraction, and the coefficient of proportionality was found to be 28.5,⁽¹²⁾ which is 37% greater than our numerical prediction of 18.

At low volume fraction, the effective viscosity as measured by the falling ball method is predicted to be given by

$$\eta_{\text{eff}} = \eta(1 + 18\Phi)$$

for suspensions of fibers of aspect ratio 20. This is quite different from the effective shear viscosity of $\eta(1 + 6.2\Phi)$ for fibers at the same aspect ratio; this difference has been observed in experiments⁽¹²⁾ and is due to the anisotropy of the fluid.

4. FINAL REMARKS

We presented the results of a numerical simulation of a steady flow generated by a sphere falling along the centerline of a cylindrical tube containing a suspension. The suspension is regarded as a continuum and is modeled by the Ericksen TIF constitutive equation.

The numerical results show that the flow is intrinsically unsteady, and the drag force depends on the initial configuration of the microstructure. However, the time variations in the drag force about its mean value and the lack of knowledge of the initial configuration of the microstructure con-

tribute only about $\pm 1\%$ uncertainty in the drag force on the sphere. For suspensions of spheroids of aspect ratio of 10, the falling sphere method is predicted to yield an effective (long-time average) viscosity of $\eta(1 + 5.8\Phi)$, whereas for suspensions of spheroids of aspect ratio 20, an effective viscosity of $\eta(1 + 18\Phi)$ is predicted. This latter prediction agrees reasonably well with the data on suspensions of blunt-ended cylinders and chopped nylon fibers of aspect ratio of about 19.8.⁽¹²⁾

Furthermore, we find that the kinematics is Newtonian-like, although a detailed look at the evolution of the microstructure along the tube reveals that there may be thin boundary layers across which the orientation vector \mathbf{p} flips its direction. The resolution of these boundary layers makes it difficult to analyze complex flows of suspensions. In the downstream region (i.e., behind the falling sphere) and at long time, the spheroids align themselves along the tube axis in agreement with some experimental observation.

The finding may be extrapolated to concentrated suspensions if it can be shown that the TIF model is an adequate continuum description for these suspensions. So far, experimental data on concentrated suspensions in simple flows are scarce; apart from the preliminary studies by Acrivos *et al.*,⁽²²⁾ there are no serious efforts to try to come up with a workable constitutive equation for concentrated suspensions. The more complicated constitutive equation proposed by Acrivos *et al.*,⁽²²⁾ with suggested parameters, has also been implemented and tested in this flow. A steady-state flow is possible, and there is no oscillation in the plot of the drag force versus time. The steady-state drag force is about 10% below the Newtonian value (using the same viscosity) at a solid concentration 55%. Whether or not a steady-state flow is physically realizable can only be determined from experiments. However, it makes sense to study a more complex model only if a simpler one (i.e., the TIF model) has been shown to be inadequate.

An alternative approach is to solve this problem as a many-body problem, for example, by the Stokesian dynamics simulation.⁽²⁹⁾ This latter technique is still in its preliminary stage, and no other numerical scheme for solving many-body problems is a viable alternative for present-day computers. The continuum approach will yield useful results in the foreseeable future.

ACKNOWLEDGMENTS

This research is funded by an Australian Research Grant Scheme. The support is gratefully acknowledged. Portions of this work were supported by a grant from the Division of Engineering and Geosciences, Office of Basic Energy Science, U.S. Department of Energy (KC04106). Work per-

formed at Los Alamos Laboratory was sponsored by the U.S. Department of Energy under contract W-7405-ENG-36 with the University of California. N. P.-T. wishes to thank the Staff of the Technical Engineering Support Group at Los Alamos for providing the facilities and support that allowed this study to be performed.

REFERENCES

1. A. Acharya, R. A. Mashelkar, and J. Ulbrecht, *Rheol. Acta* **15**:454 (1976).
2. R. B. Bird, O. Hassager, and R. Armstrong, *Dynamics of Polymeric Liquids: Vol. I, Fluid Mechanics*, 2nd ed. (Wiley, 1988).
3. K. Adachi, N. Yoshioka, and K. Sakai, *J. Non-Newtonian Fluid Mech.* **3**:107 (1977/1978).
4. G. Tiefenbruck and L. G. Leal, *J. Non-Newtonian Fluid Mech.* **10**:115 (1982). 115.
5. Gu Dazhi and R. I. Tanner, *J. Non-Newtonian Fluid Mech.* **17**:1 (1985).
6. O. Hassager and C. Bisgaard, *J. Non-Newtonian Fluid Mech.* **12**:153 (1983).
7. X.-L. Luo and R. I. Tanner, *J. Non-Newtonian Fluid Mech.* **21**:179 (1986).
8. M. J. Crochet, Paper presented at the X International Congress of Rheology, Sydney (1988), No. 19.
9. R. Brown and R. C. Armstrong, Paper presented at the Sixth Workshop on Numerical Methods in Non-Newtonian Flows, Denmark (June 1989).
10. F. Sugeng and R. I. Tanner, *J. Non-Newtonian Fluid Mech.* **20**:281 (1986).
11. Fifth Workshop on Numerical Methods in Non-Newtonian Flows, *J. Non-Newtonian Fluid Mech.* **29**:ix (1988).
12. W. J. Milliken, M. Gottlieb, A. L. Graham, L. A. Mondy, and R. L. Powell, *J. Fluid Mech.* **202**:217 (1989).
13. R. L. Powell, Paper presented at the Workshop on Dynamics of Concentrated Systems, Center for Nonlinear Studies, Los Alamos (June 1989).
14. R. Zheng, N. Phan-Thien, and R. I. Tanner, Paper presented at the 6th Workshop on Numerical Methods in Non-Newtonian Flows, Denmark (June 1989); *J. Non-Newtonian Fluid Mech.* **36**:27 (1990).
15. J. L. Ericksen, *Arch. Rat. Mech. Anal.* **3**:117 (1960).
16. G. K. Batchelor, *J. Fluid Mech.* **41**:545 (1970).
17. R. G. Cox and H. Brenner, *Chem. Eng. Sci.* **26**:65 (1971).
18. L. G. Leal and E. J. Hinch, *J. Fluid Mech.* **46**:685 (1971).
19. L. G. Leal and E. J. Hinch, *Rheol. Acta* **12**:127 (1973).
20. G. G. Lipscomb II, M. M. Denn, D. U. Hur, and D. V. Boger, *J. Non-Newtonian Fluid Mech.* **26**:297 (1988).
21. G. B. Jeffrey, *Proc. R. Soc. Lond. A* **102**:161 (1922).
22. A. Acrivos, D. J. Jeffrey, F. Gadala-Maria, and E. Herbolzheimer, Final Report, AF-1085, Research Project 314-1, Stanford University, Chapter 3 (1979).
23. Y. Ivanov, T. G. M. Van de Ven, and S. G. Mason, *J. Rheol.* **26**:213 (1982).
24. E. Ganani and R. L. Powell, *J. Rheol.* **30**:995 (1986).
25. N. Phan-Thien, F. Sugeng, and R. I. Tanner, *J. Non-Newtonian Fluid Mech.* **24**:97 (1987).
26. U. Heise, *Comp. Meth. Appl. Mech. Eng.* **28**:145 (1981).
27. S. J. Karrila and S. Kim, *Chem. Eng. Commun.* (1989), in press.
28. J. Happel and H. Brenner, *Low Reynolds Number Hydrodynamics* (Noordhoff, Leiden, 1973).
29. J. F. Brady and G. Bossis, *Annu. Rev. Fluid Mech.* **20**:111 (1988).